A Comparative Study of Lidar and Camera-based Lane Departure Warning Systems

Jordan Britt, Christopher Rose, David M. Bevly

Auburn University

ABSTRACT

This paper presents a comparison of a lidar and camera based lane departure warning methods. The two methods are analyzed based on their ability to determine the position of the vehicle in the lane under various weather and lighting scenarios. The position of the vehicle reported by the vision systems is compared to a precision survey of the lane markings at the National Center for Asphalt Technology (NCAT) test track and an RTK position of the vehicle. The criteria used to assess the performance of the two methods are based on detection rates, position error, and position variance.

INTRODUCTION

Nearly half of all highway fatalities occur from unintended lane departure warnings which comprise nearly 20,000 deaths annually [1], [2]. The most basic form of a lane departure warning system is one that will determine the lateral position of the vehicle within the lane. Using this information a system can be designed to alert the driver when they are expected leave the lane of travel. These systems often distinguish between intentional lane departures and unintentional lane departures on whether a turn signal was used. Additionally, when these sensors are used in conjunction with a map of the lane markings and a GPS, greater position accuracy can be achieved, as well as provide information to make it possible to use GPS with a reduced number of satellites [3].

Most lane departure warning systems typically use either a lidar (Light Detection and Ranging) or a camera to detect the lane markings [4], [5], [6], [7]. A lidar is a laser scanner that will typically report both a range between the lidar and the surface the laser is contacting as well as a measure of reflectivity of that surface. This measurement of surface reflectivity is know as echowidth. It is this measurement that will be used to detect the lane markings on the basis that lane markings should have an increased reflectivity above the road surface.

Camera-based lane departure and detection systems are well developed, and units are available on commercial vehicles. In literature, one LDW system, by Jung and Kelber [8], used a linear-parabolic model to create a lane departure warning system using lateral offset based on the near field and far field. For the near field close to the camera's position in a forward looking camera, a linear function was used to capture the straight appearance of the road close to the car, and for the far field, a parabolic model was used to model the curves of the road ahead. In their following paper [9], Jung and Kelber used their system with the linear-parabolic model to compute the lateral offset without camera parameters. In [10], optical flow was used to achieve lane recognition under adverse weather conditions. Feng [11] used an improved Hough transform to obtain the road edge in a binary image, followed by establishment of an area of interest based on the prediction result of a Kalman filter. In [12], an extended Kalman filter was used to model the lane markings to search within a specified area in the image so that far lane boundaries are searched with a smaller area than closer lane boundaries, thus reducing the impact of noise. The approach of [13] calculated the heading from the image based on the vanishing point of the measured lane markings and the vanishing point of the camera. The vanishing point of the measured lane markings is the point in the image where the lane markings meet given a straight road.

The ability of both the camera and lidar to detect lane markings and report the position of the vehicle in the lane will be compared over a range of varying scenarios that were chosen to be the most likely to be incurred while driving. These scenarios look at performance during driving at noon, dusk, night, and rain. A precision survey of the lane markings at the NCAT test track is compared to an RTK GPS position of the vehicle to provide a highly accurate measurement of sensor performance.

OVERVIEW OF HARDWARE

The three key sensors used in this particular research are a laser scanner, a camera, and a GPS receiver. All aforementioned sensors were mounted on the roof of the test vehicle, a 2007 Infiniti G35 Sedan. Specifically the lidar and camera where mounted on the center of a roof-rack cross bar. They were both positioned so that they were downward facing with a pitch of approximately 22 degrees. The GPS antenna was mounted six inches behind the lidar and camera along the centerline of the vehicle.

Lidar

Lidars are an active sensor meaning that they actively transmit and receive a signal (a laser in this case) to perceive their environment whereas a camera would be a passive sensor, merely receiving environmental information. The specific lidar used is an Ibeo Alasca XT, which is an automotive grade multi-layer lidar. Specifically, this lidar has 4 layers as seen in Figure 1 which have a maximum vertical divergence of 1.6°, 0.8°, -0.8°, and -1.6°. Additionally, this lidar reports both a distance as well as a reflectivity measurement to the contacting surface. This research operated the lidar at a rate of 10Hz which yielded a horizontal angular resolution of 0.25°. Additionally this lidar is a multi-echo device, meaning that if the laser passes through another object and contacts a second object a measurement of both distance and reflectivity to the first and second object will be reported. The lidar is capable of reporting these multiple echoes for up to four objects, allowing it to be more robust to the affects of precipitation than lidars without this technology.
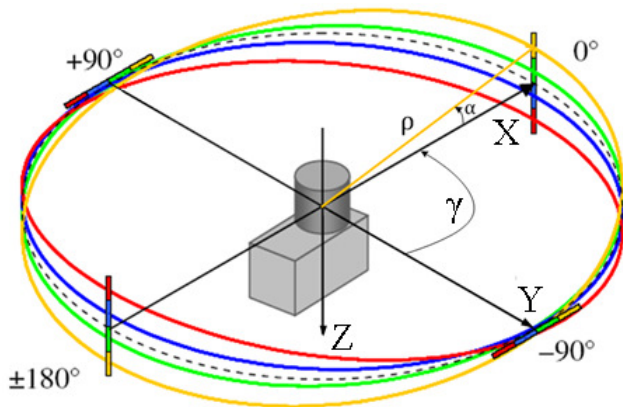

Figure 1. Ibeo Lidar

Camera

The webcam, a QuickCam Pro 9000 selected for this testing, is a low cost, consumer grade webcam. The resolution used for lane detection was very low at 244x108 pixels, and the frames per second were about 10Hz.

GPS

The specific GPS used in this research was a Novatel ProPak-V3. This GPS was used in conjunction with the Alabama Department of Transportation (ALDOT) Continuously Operating Reference Stations (CORS) Network, which provides RTK correction to obtain centimeter level accuracy with GPS. The ALDOT CORS Network was also utilized during the survey of the lane markings so that their precise position could be known, thus allowing for the computation of a highly accurate position in the lane.

LIDAR BASED LDW METHOD

An overview of the specific lidar based lane detection algorithm is provided below. A more in-depth description of this method can be found in [14]. Most common algorithms for lane detection are based off of histograms, where the lane is quantized into various small areas, the reflectivity in that area is averaged and used to generate a histogram, and lanes are detected by being above a certain threshold of reflectivity [15], [16], [17]. The method analyzed here is one based off matching a dynamic lane model to the data captured by the lidar.

Before the lane model can be generated, the area in which the lidar is capable of scanning is bounded. This bound is defined as an area large enough where if the left tires are contacting the left lane markings, the right lane marking is still capable of being scanned. Hence, this bound guarantees that a lane marking will be scanned if it is present as seen in Figure 2. By reducing the search area, this bound also allows for reduced processing time as well as potentially removing objects that could be mistaken for lane markings. Now that this bound has been established, the first step of generating the lane model is scanning the area directly in front of the vehicle as seen in Figure 2 in green. This step assumes that the vehicle is not currently over a lane marking and is used to determine an average reflectivity measurement of the lane.
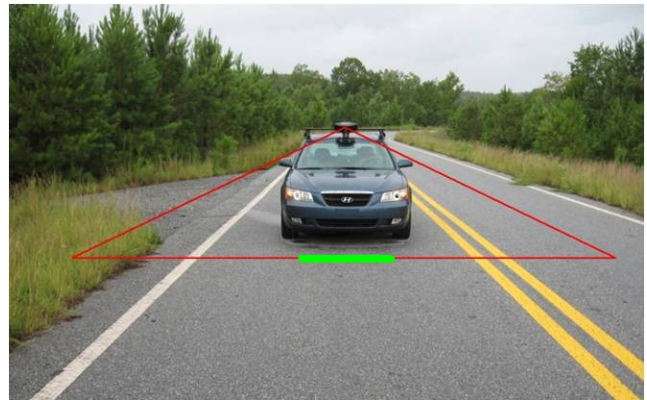
Figure 2. Lidar Bound

This average reflectivity is used to model the road surface. The lane markings are then modeled as a 75% increase in reflectivity over this average reflectivity. This model is shown in Figure 3. This lane model is then matched to the lidar data by calculating the minimum mean square error between the lane model and the lidar scan. During this minimum mean square error calculation the lane model width varies from some minimum lane width to some maximum lane width in

increments of the horizontal resolution of the lidar. Once the lane model is matched to the lidar data, the area where the model lane markings and the actual lane markings should overlap is analyzed. If the reflectivity from where the lane markings are thought to be located are not at least 30% more reflective than the average road surface used to generate the lane model, the conclusion is drawn that lane markings do not actually exist at this location with great enough certainty to use this measurement, and it is ignored. Assuming that this test is passed, a narrowed search band of approximately four degrees is placed around the location of this lane marking so that future searches have a further narrowed search. If the test fails twice, this narrowed search area is dropped in favor of the original larger search area.
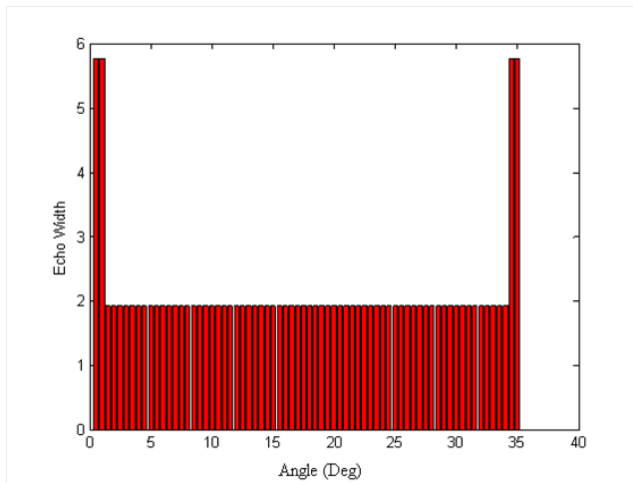

Figure 3.   Lane Model

When a lane marking is detected, the lateral position in the lane is calculated. The position in the lane in this context is a measurement of the distance from the vehicle to the center of the lane, where if the vehicle is to the left of this centerline the distance is negative, and if the vehicle is to the right of this centerline, the distance is positive. Hence if both the left and right lane markings have been detected, is it simply a matter of averaging these two distances to determine the position of the vehicle in the lane. If only one lane marking is detected, the position of the vehicle in the lane can still be detected; however, a lane width must be assumed. This assumed lane width can be from either a measurement from when both lane markings were detected or from an ideal lane width. In this case the unknown measurement between the vehicle and the lane markings is calculated by subtracting the known measurement from the lane width. The position in the lane is then calculated as previously mentioned. Once the position of the vehicle in the lane has been calculated, the result is filtered using a single state Kalman filter to simply smooth the data, thereby mitigating any erroneous jumps in position due to false detections.

CAMERA-BASED LANE SYSTEM

The camera-based lane detection system detects the lane markings within the image, creates a measurement for the 2nd

order polynomial model for the lane markings, and determines the heading and lateral distance to the lane marking. A linear Kalman filter estimates the coefficients of the polynomial model to reduce the impact of erroneous lane model measurements. The lane marking detection procedure can be seen in Figure 4, and much of the algorithm can be found in [7].
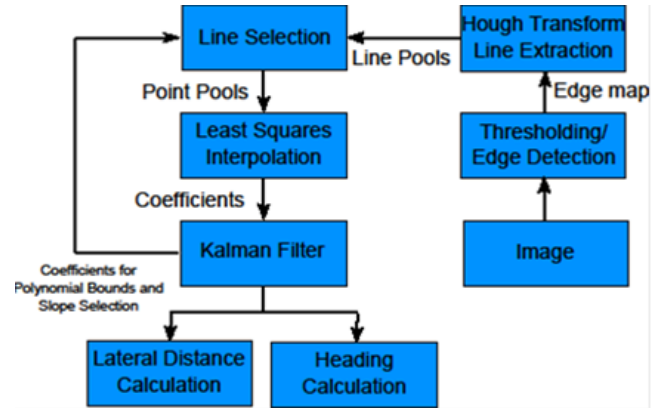

Figure 4.   Block Diagram of Camera System

Image processing

Following calibration of the camera and image correction in order to ensure the assumption of no skew and lens distortion in the pinhole camera model, a histogram-based thresholding procedure was conducted to eliminate unwanted features from the image and emphasize desired features. The threshold is chosen using the mean and standard deviation of the image where T = threshold, μ = mean, K = chosen noise value, and σ = standard deviation of image.

$$T = \mu + K\sigma \qquad (1)$$

A histogram of the image provides a basis for the determination of the thresholding needed to extract the lane markings from the image. Brighter colors, such as white and yellow, are typically on the higher end of an image's histogram. As such, extraction of the lane markings from the image can be achieved by choosing a threshold which is close to the upper end of the grayscale range. However, the grayscale value which constitutes the upper end of the grayscale range can change due to varying environments. For example, Figure 5 shows the thresholded image for a constant threshold of 210 (a good threshold for day environments) in a dark environment and the thresholded image for a dynamically chosen threshold based off of the histogram of the image. The lane markings are clearly visible in the dynamically thresholded image.

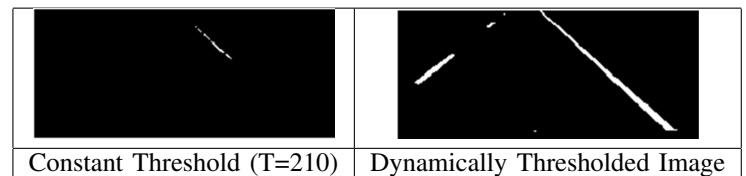| Constant Threshold (T=210) | Dynamically Thresholded Image |

Figure 5.   Image for Various Thresholds

After thresholding, Canny edge detection and the Hough transform are employed to extract lines from the image. The parameters for the Hough transform were chosen such that lines were fairly long and breaks in the lines were removed.

Lane model determination

Two additional criteria are needed to reduce the number of non-lane marking lines extracted from the Hough transform. Lines from the Hough transform are chosen such that they lie in close proximity (in the image space sense) to the current polynomial model as well as having a slope which is close to the slope at the nearest point on the current polynomial model curve. Figure 6 shows the lines which pass these two criteria (blue) and those lines that fail the criteria (red) from shadows on the road. The chosen lines are then separated into right and left lane marking using their slopes, and left and right lane marking point pools are created using the endpoints and midpoint of the lines in the respective line pools.

Figure 6. Hough Lines (red-ignored, blue-selected)

The left and right lane marking point pools both undergo a least squares 2nd-order polynomial interpolation for a measurement of the lane model. This measurement is then used in a simple linear Kalman filter, whose measurement noise covariance matrix determines the amount by which the estimate of the model is affected by the measurement. Erroneous measurements of the model, then, are filtered and their effect reduced.

Heading and Lateral Distance Calculation

With the estimate of the lane markings, the heading of the vehicle with respect to the lane markings is found by comparing the vanishing point of the image with the vanishing point of the lane markings. The heading is calculated using Equation 2 where OP is the distance in pixels from the image vanishing point to the vanishing point of the lane marking, θ is the visual angle of the camera, and OP_2 is the distance in pixels from the image vanishing point to the edge of the image [13]. Figure 7 shows the corresponding variables required for the heading calculation. Due to testing being conducted primarily on straight roads, this heading measurement has little effect on the distance from lane center calculation, since the heading is close to 0 for most data runs.

$$\psi = \arctan{(\vec{OP}\frac{\tan\frac{\theta}{2}}{\vec{OP_2}})} \qquad (2)$$

The distance from lane center measurement is determined using the vanishing point of the lane markings when the vehicle is perfectly straight in the road and the locations of
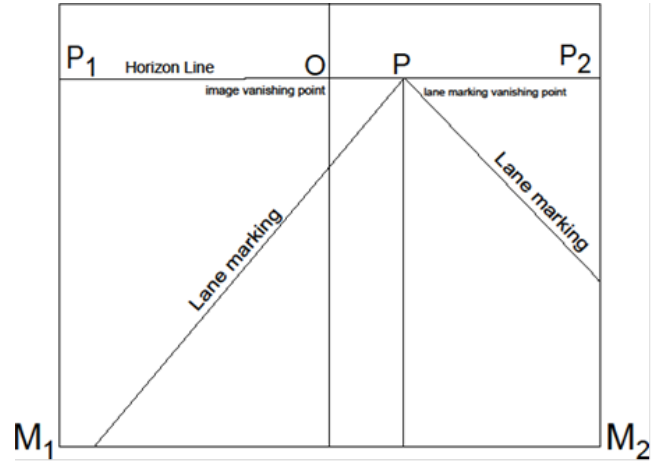

Figure 7. Heading Calculation from Image

the estimated lane markings in the image. The number of pixels from the vanishing point of the lane markings and the estimated lane marking determines the lateral distance to the lane marking using Equation 3 where a, b, and c are the coefficients of the lane marking, y is the lowest row of pixels in the image, and n is the conversion factor from pixels to real units corresponding to the lowest row of pixels in the image.

$$d_r = n(\frac{-b+\sqrt{4ay+b^2-4ac}}{2a})$$
$$d_l = n(\frac{-b-\sqrt{4ay+b^2-4ac}}{2a}) \qquad (3)$$

This conversion factor assumes that the pinhole camera model has no skew or lens distortion and remains constant over the extent of the row of pixels. To determine the distance from lane center, both lane markings provide the location of the center of the lane in the image. When only one lane marking is known, the lane width is assumed to be 3.658 meters, and the lateral distance is subtracted from half of the lane width to determine the lateral distance from the center of the lane. Any alterations due to mounting (heading misalignment / offset from center of vehicle) can be compensated here as well.

TESTING

The lidar and camera based methods were analyzed under a number of different scenarios chosen to be representative of the kinds of scenarios a driver is most likely to encounter while driving. These include the following scenarios: driving during noon, dusk, night, and afternoon hours, departing and returning to the lane, and night in both low beam and high beam as well as analyzing the effects of oncoming traffic in either low beam or high beam.

Testing was performed at the National Center of Asphalt Testing (NCAT) in Opelika, Alabama as seen in Figure 8. The test track is a two lane 1.8 mile oval with eight degrees of bank in the turns and is sectioned off with various types of asphalt which are currently at the end of their lifetime. As such, the track represents a challenging environment for any lane detection algorithm due to areas of changing asphalt as seen in Figure 9, missing or occluded lane markings as seen in Figure 10, off ramps as seen in Figure 11, and rumble strips

also seen in Figure 10 while still maintaining a very realistic representation of highway driving.
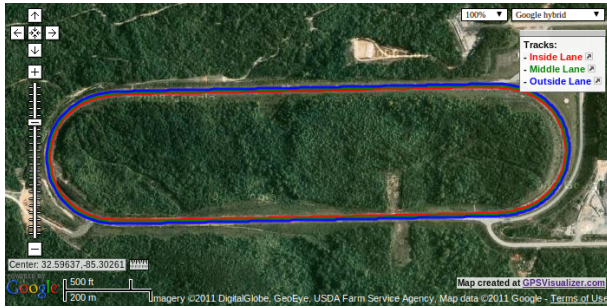

Figure 8.   NCAT Test Track

Dashed lane markings separate the two lanes with solid lane markings denoting the inside and outside most lane marking. A precision survey of each dashed lane marking and the adjacent solid lane marking were taken for the entirety of the track. The mid-point of each lane was then calculated by simply finding the midpoint of the dashed lane markings survey and the corresponding solid lane markings survey. This survey can be seen pictorially in Figure 12 where the green lane denotes the dashed lane survey, the red the solid lane survey, and the blue the center of the lane. The distance between the centerline of the lane and the position of the vehicle as determined by RTK GPS will be compared to the output of the camera and lidar lane detection algorithms. Where if the vehicle is to the right of centerline it will be denoted as a positive distance and if the vehicle is to the left of the centerline, it will be denoted by a negative distance.

Figure 9.   Various Asphalts on Test Track

The test procedure consisted of driving approximately 55mph and logging RTK GPS, lidar and camera data. The aforementioned speed was selected to meet the soft speed limit of the track while still maintaining a speed representative of highway driving. Approximately 9 miles of data was gathered from each scenario. This data was post-processed with the turns neglected due to their sharp turns and large bank angles being unrepresentative of typical highways. This mitigates

Figure 10.   Missing Lane Markings

Figure 11.   Off Ramp

any errors in our results due to super elevation and the like. The results are analyzed on the basis of mean absolute error (MAE), mean square error (MSE), the standard deviation of the error (σ_{Error}), and detection rates (%Det). It is worth noting that both the dashed and solid lane markings are white, and while the outside lane marking is not always present, the dashed lane markings are always present.

Afternoon

The afternoon testing comprised testing between the hours of 12:00pm and 3:00pm. This specific test was analyzed to provide a baseline of system performance where the effects of shadows or poor lighting would be minimized. These tests occurred as speeds of 35, 45, and 55 MPH to assess if a change in speed had an appreciable affect on performance as seen in Table I. From these tests it can be inferred that under normal circumstances the lidar has a mean average error of approximate 0.1m. It is worth noting that the detection rates presented here are actually slightly lower than those of the other potentially non-ideal scenarios. This is most likely due to this data set actually being the last scenario where
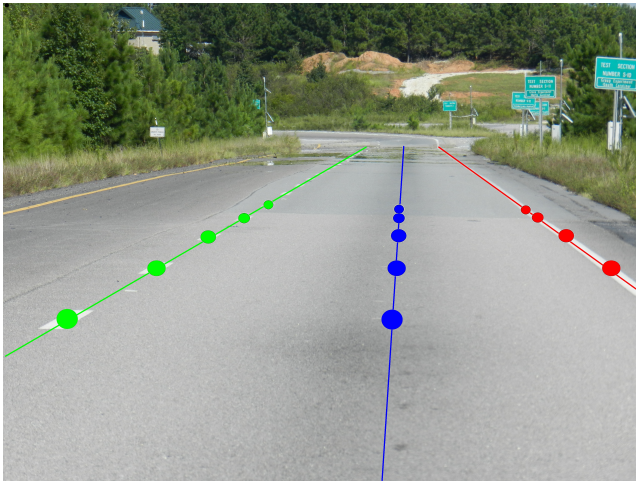
Figure 12. Lane Survey and Midpoint Locations

data was collected and there being a small accumulation of dust and bugs on the lidar causing a slightly reduced rate of detection. Note this data set contains shadows crossing the road from the trees along the road. Most of these shadows did not significantly effect the results; however, the low lying sun created problems similar to the dusk datasets for the afternoon data runs for the camera.

Table I
VARIOUS SPEEDS AFTERNOON

	Scenario	MAE	MSE	σ_{Error}	%Det
Lidar	35 MPH	0.1070	0.0233	0.1508	88
Camera	35 MPH	0.0453	0.0031	0.0399	51
Lidar	45 MPH	0.0991	0.0179	0.1265	92
Camera	45 MPH	0.0595	0.0052	0.0533	46
Lidar	55 MPH	0.1124	0.0240	0.1482	95
Camera	55 MPH	0.0699	0.0066	0.0456	55

Noon Weaving

These tests occurred between 12:00pm and 1:00pm and consisted of departing and returning to the lane along various points along the track. The first test was conducted at various speeds and consisted of driving approximately 35mph in the turns and accelerating to 55mph in the straights. The results are shown in Table II. The other tests were conducted at constant speeds of 40 and 30MPH to see if an appreciable change in performance occurred at varying speeds.

While the lidar did not show any appreciable change in detection rates throughout the runs there is a noticeable change in the mean absolute error in the 30 MPH. This change is due to the large yaw angles of the vehicle encountered when the vehicle turns in and out of the lane to avoid other vehicles. This departure angle is often reduced a higher speeds; hence, the other test scenarios do not reflect this error.

The accuracy of the camera results for the noon test runs stayed fairly consistent over the course of the run. Nevertheless, the degraded edges of the lane marking, as seen in Figure 13, as well as the completely missing solid lane markings affects the detection rate of the camera lane detection system.

Since the camera algorithm extracts edges from the image, the degraded lane marking fails to produce an edge for the lane marking. In these situations, the camera algorithm typically detects either the other side of the lane marking that does not have the degradation or no lane marking at all.

Figure 13. Degraded Lane Marking

Typical problems for camera lane detecting during the noon test data that would have problems on a typical road but are not seen in the test results involve tracking of features in the image that are similar to the lane marking but are not actually the desired tracked lane markings. For example the off ramp's lane marking branches off of the road. Since no lane marking exists at the off ramp, the feature tracking typically tracks the off ramp lane marking, which causes erroneous distance to lane center and heading measurements. In addition, as the road's lane markings come back into view, the off ramp's left lane marking can provide lines along with the road's lane marking, resulting in a lane estimate between the off ramp lane markings and the road's lane markings. Figure 14 shows this effect from the camera image.

Figure 14. Effect of off ramp on camera algorithm

As seen in Figure 14, the black lines correspond to the polynomial boundary lines for line selection, the thick red line represents an estimate of the lane marking location that is not detected for the current frame, a thick green line represents an estimate of the lane marking location that is detected for the current frame, a thin red line represents a line from the Hough transform that is ignored due to the two selection criteria, and a thin blue line corresponds to a line from the Hough transform

that passes both selection criteria. Both sides of the road's right lane marking is detected as well as the left edge of the off ramp's lane marking. These three lines (blue) result in an estimate of the lane marking that lies between the road's lane marking and the off ramp's lane marking. This effect is magnified at lower speeds since more frames with the off ramp present in the image results in further tracking of the erroneous off ramp.

Throughout the data runs, the right lane marking was the primary tracked lane marking. The dashed center lane marking was typically detected in the noon runs as well as the more ideal data runs, but these detections were only 1-2 frames and were ignored. Due to the minimum line length parameter from the Hough transform, the dashed lane markings further down the road were not detected, and only the dashed lane markings that were close to the vehicle were detected. A smaller minimum Hough transform parameter would increase the detection of the dashed lane marking at the expense of more noisy lines in the image.

The camera algorithm was tuned to emphasize the rejection of false positives with the drawback of increased misses. Past testing in very noisy environments has shown that consistent erroneous line detections from image to image can cause failed tracking of the lane marking, which, due to the selection criteria, results in further failed tracking once the polynomial boundary lines fall outside of the lane markings. As such, the emphasis on the rejection of false positives reduces catastrophic lane estimate failures at the cost of increased misses.

Table II
NOON WEAVING

	Scenario	MAE	MSE	σ_{Error}	%Det
Lidar	Var	0.1202	0.0287	0.1686	100
Camera	Var	0.0872	0.0123	0.0761	71
Lidar	40 MPH	0.1818	0.1108	0.3076	98
Camera	40 MPH	0.1077	0.0511	0.2246	80
Lidar	30 MPH	0.2081	0.1566	0.3649	100
Camera	30 MPH	0.0717	0.0128	0.1018	82

Dusk

Dusk testing ranged from one hour to thirty minutes before sunset. Due to the alignment of the track with the cardinal directions, the vehicle drove west (into the sun) on one straight and east (away from the sun) on the opposing straight. These tests where conducted primarily as a way of analyzing if the either the camera or the lidar noticed any appreciable change in performance due to either being blinded by the sun or shadows on the roadway. The first test occurred approximately one hour before sunset at a speed of 55mph, the second test occurred 45 minutes before sunset at 45mph, and the final test occurred 30 minutes before sunset at 30mph. The results of which can be seen in Table III.

Throughout the tests the lidar appears to be largely unaffected by either speed or changes in ambient lighting. This result is most likely due to the fact that the lidar is an active sensor and therefore should be largely unaffected by shadows on the roadway. Additionally while a lidar is capable of being

washed out by the sun, an error known as dazzling, this would most likely occur when a vehicle was cresting a hill during dusk, such that the sun would be more incident on the downward facing lidar. However, due to the flatness of the test track, this situation did not occur.

The detection rate of the camera algorithm for the dusk data was lower than that for the noon data sets. Driving at the sun caused the camera to wash out as seen in Figure 15. For the length of the straight track facing west, the camera fails to detect a lane marking, as shown by the red lines (no detection for the frame for the lane marking). The dynamic threshold algorithm essentially pushes the threshold beyond the actual threshold for the lane markings due to the impact of the sun and sun rays on the histogram of the image. As such, the threshold operation removes the lane marking, and the algorithm has no chance of detecting the lane marking. As the vehicle turns away from the sun and drives into the shadow of the trees, the lane markings are immediately detected.
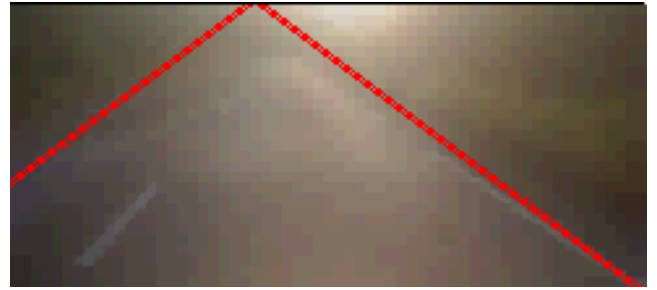

Figure 15. Failure to detect lane markings at dusk when facing the sun

Table III
TESTING DURING DUSK

	Scenario	MAE	MSE	σ_{Error}	%Det
Lidar	1hr	0.1113	0.02	0.1156	100
Camera	1hr	0.1233	0.0515	0.2269	59
Lidar	45min	0.0967	0.0176	0.1245	100
Camera	45min	0.1021	0.0592	0.2433	57
Lidar	30min	0.0889	0.0113	0.1007	100
Camera	30min	0.0657	0.0068	0.0636	55

Rain

Rain testing occurred during daylight hours and was conducted as Auburn experienced remnants of a tropical storm. The first scenario labeled "Light" was data taken just as the rain began and was little more than a sprinkle. The final scenario labeled "Heavy" was taken at the peak of the downpour where it became difficult for the driver to distinguish the lane markings. The scenario labeled "Medium" was simply the data set that occurred between "Light" and "Heavy" as determined simply as a function of time. The results of which can be seen in Table IV. All tests where performed at 55MPH with the windshield wipers engaged.

The performance of the lidar based algorithm is acceptable in the light rain scenario and continues to produce reasonable errors even in the medium rain scenario albeit with a significantly reduced detection rate. However during the heavy

downpour, the lidar is rendered virtually useless only detecting a lane marking one-percent of the time and even then with significant error.

	Scenario	MAE	MSE	σ_{Error}	%Det
Lidar	Light	0.0962	0.0146	0.1205	92
Camera	Light	0.0840	0.0106	0.0733	92
Lidar	Medium	0.1046	0.0177	0.1314	65
Camera	Medium	0.0885	0.0101	0.0635	91
Lidar	Heavy	0.7805	0.7921	0.4682	1
Camera	Heavy	0.0795	0.0089	0.0670	53

Night

The night scenarios where conducted to determine the performance of the algorithms in low light situations, specifically to see if the reduced natural lighting mitigated errors caused by shadows might affect the camera as well as to see if the headlight provided sufficient illumination for lane detection in both high and low beam situations. Additionally the affects of oncoming traffic in both high beam and low beam were analyzed. All data was collected at 55mph.

High / Low Beam: The results from driving with the test vehicle lights in low and high beam settings are presented in Table V. Note that in addition to stripes in the center lane, the center lane also contained LED road reflectors. Based on these results it would appear that the performance of the lidar based algorithm is unaffected by having the headlights in either the high or low beam condition or night driving in general. The camera algorithm at night presents a more ideal scenario for the camera algorithm since many of the features that could cause unwanted tracking, such as billboards, guardrails, and other objects, are easily thresholded due to the darkness in the image. The headlights of the vehicle illuminate the road and provide the dynamic threshold operation with a histogram which can easily determine a valid threshold value to detect the lane markings.

	Scenario	MAE	MSE	σ_{Error}	%Det
Lidar	High Beam	0.1012	0.0168	0.1208	100
Camera	High Beam	0.3154	0.1597	0.3503	86
Lidar	Low Beam	0.0966	0.0159	0.1215	99
Camera	Low Beam	0.1182	0.0185	0.0762	84

Oncoming Traffic in Low / High Beam: For the oncoming traffic tests a Hyundai Santa Fe was parked in the adjacent lane facing the vehicle to simulate oncoming traffic. For the first round of testing the headlights of the vehicle were in the low beam position. For the second set of testing the headlights were in the high beam position. For both tests, the headlights of the test vehicle were in the low beam position. Several laps where driven at the vehicle so that an average performance of the algorithms could be established. Figures 16 and 17 show the results from the low and high beam test respectively. The closing distance is defined as the distance between the test

vehicle and the static vehicle where approaching the static vehicle constitutes a positive closing distance, and any distance past the static vehicle constitutes a negative closing distance. In an effort to generate legible figures, data from all the runs was quantized into 10m section of closing distance and averaged.

Notice that the lidar based algorithm appears to determine the distance of the vehicle in the lane with a similar level of accuracy as the noon data runs for the majority of the exercise. However, in Figure 17 there is a noticeable spike in the lidar based position error just as the lidar is next to the vehicle. This error is actually not caused by the oncoming headlights of the vehicle, but rather by the lidar actually scanning the oncoming vehicle and detecting the vehicle as a lane marking.

The results for the oncoming car data for the camera algorithm were actually surprising given past tests with oncoming headlights. Headlights in the image can act like the presence of the sun, where the histogram pushes the calculated threshold above a threshold which can detect the lane markings. In this scenario, the oncoming vehicle had headlights which were dimmer than a typical vehicle, and thus the impact of the headlights was decreased. Note that the gaps in camera detection seen at -200m closing distance in both runs is due to an area of the track where the solid lane markings is not present as seen in Figure 10. The lidar here reported a position based off the dashed lane markings.
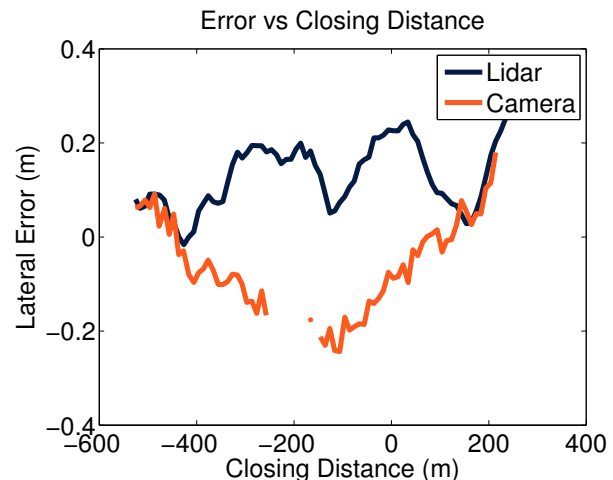

Figure 16. Oncoming Vehicle in Low Beam

CONCLUSIONS AND FUTURE WORK

If the single worst data run from the camera and the lidar was removed and all the results averaged, the camera out-performs the lidar by 4cm on average; however, it also detects a lane marking 27% less often on average. It is worth noting that the width of standard lane marking is 15.25cm (6 inches); therefore, with measurement differences this small it becomes an issue of where an algorithm detects the lane marking, be it an edge or center of the lane marking. However, based on the results presented it is clear that the lidar based algorithm performs poorly in moderate to heavy rain, as well as when directly next to other vehicles. However the lidar based algorithm appears largely unaffected by changes in
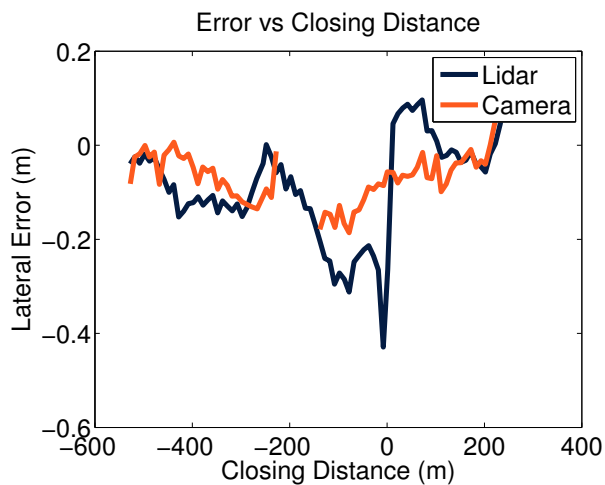
Figure 17.   Oncoming Vehicle in High Beam

camera algorithm's performance in the rain since the sloshing effect is minimized, and the rain's effect would be limited to raindrops and water on the road.

lighting or speed. The standard deviations for most of the runs are similar throughout the test scenarios. The percent detections for the camera based scenarios of noon, rain, and night are around 75% detections. On the afternoon runs, the sun was low in the horizon, and the lane markings could not be detected by the camera based system as was seen in the dusk runs.

The biggest drawback to the camera algorithm is the detection rate of the lane markings. Despite the presence of eroded lane markings and completely eliminated solid lane markings, the camera algorithm still failed to detect lane markings in images where lane markings could be detected. The tuning of the camera algorithm was intended to reduce the number of false positives at the expense of increased misses. Several factors are present which can reverse this result. The Hough transform parameters provide a means for reducing the minimum line length, which will result in increased lines in the image, more line pools, and especially in the case of the dashed lane markings, more detections. However, with smaller lines, the lines could also be a result of non lane marking lines. The dynamic threshold is a very important step in the lane detection algorithm. With a smaller chosen K value (or the scalar on the standard deviation), the camera algorithm could more likely detect the lane markings in the presence of the sun and other bright features since the calculated threshold is lower. Finally, the Kalman filter in the current iteration is more conservative than the true dynamics of the vehicle, and the lane marking estimate can lag behind the true lane marking in the image when the vehicle is shifting quickly within the lane.

Webcams also typically have significant distortion, which can effect the center to lane measurements. Certainly, with a higher end camera, the results, both in accuracy as well as detection rate, could improve. Additionally, by moving the camera to the inside of the vehicle, exposure to the elements could be prevented. For example, the sloshing of the rain on the camera during the rain data could be minimized at the cost of sloshing on the windshield. Also, a simple cover to fully protect the camera from rain could significantly improve the

REFERENCES

[1] U. S. D. of Transportation Federal Highway Administration. (2010, January) Roadway departure safety. Online. [Online]. Available: http://safety.fhwa.dot.gov/roadway_dept/#facts

[2] F. S. Barickman, "Lane departure warning system research and test development," *Transportation Research Center Inc.*, no. 07-0495, 2007.

[3] D. B. John Allen, "Use of vision sensors and lane maps to aid gps/ins under a limited gps satellite constellation," in *ION GNSS*, 2009.

[4] S. Kammel and B. Pitzer, "Lidar-based lane marker detection and mapping," in *Proc. IEEE Intelligent Vehicles Symposium*, Jun. 4–6, 2008, pp. 1137–1142.

[5] J. W. Allen, J. H. Britt, C. J. Rose, and D. M. Bevly, "Intelligent multi-sensor measurements to enhance vehicle navigation and safety systems," *International Technical Meeting of the Institute of Navigation*, pp. 74–83, 2009.

[6] J. H. Britt and D. M. Bevly, "Lane tracking using multilayer laser scanner to enhance vehicle navigation and safety systems," *International Technical Meeting of the Institute of Navigation*, pp. 629 – 634, 2009.

[7] C. Rose and D. M. Bevly, "Vehicle lane position estimation with camera vision using bounded polynomial interpolated lines," *International Technical Meeting of the Institute of Navigation*, pp. 102 – 108, 2009.

[8] C. R. Jung and C. R. Kelber, "A lane departure warning system based on a linear-parabolic lane model," in *Proc. IEEE Intelligent Vehicles Symp*, 2004, pp. 891–895.

[9] C. Jung and C. Kelber, "A lane departure warning system using lateral offset with uncalibrated camera," in *Intelligent Transportation Systems, 2005. Proceedings. 2005 IEEE*, sept. 2005, pp. 102 – 107.

[10] A. Gern, R. Moebus, and U. Franke, "Vision-based lane recognition under adverse weather conditions using optical flow," in *Proc. IEEE Intelligent Vehicle Symp*, vol. 2, 2002, pp. 652–657.

[11] Y. Feng, W. Rong-ben, and Z. Rong-hui, "Based on digital image lane edge detection and tracking under structure environment for autonomous vehicle," in *Proc. IEEE Int Automation and Logistics Conf*, 2007, pp. 1310–1314.

[12] A. Takahashi and Y. Ninomiya, "Model-based lane recognition," in *Proc. IEEE Intelligent Vehicles Symp.*, 1996, pp. 201–206.

[13] E. C. Yeh, J.-C. Hsu, and R. H. Lin, "Image-based dynamic measurement for vehicle steering control," in *Proc. Intelligent Vehicles '94 Symp*, 1994, pp. 326–332.

[14] J. H. Britt, "Lane detection, calibration, and attitude determination with a multi-layer lidar for vehicle safety systems," Master's thesis, Auburn Univeristy, 2010.

[15] J. Kibbel, W. Justus, and K. Furstenberg, "Lane estimation and departure warning using multilayer laserscanner," in *Proc. IEEE Intelligent Transportation Systems*, Sep. 13–15, 2005, pp. 607–611.

[16] K. Dietmayer, N. Kämpchen, K. Fürstenberg, J. Kibbel, W. Justus, and R. Schulz, *Advanced Microsystems for Automotive Applications 2005*, ser. VDI-Buch.   Springer Berlin Heidelberg, 2005.

[17] P. Lindner, E. Richter, G. Wanielik, K. Takagi, and A. Isogai, "Multi-channel lidar processing for lane detection and estimation," in *Proc. 12th International IEEE Conference on Intelligent Transportation Systems ITSC '09*, Oct. 4–7, 2009, pp. 1–6.